NJC

New Journal of Chemistry

An international journal of the chemical sciences

www.rsc.org/njc

Volume 32 | Number 7 | July 2008 | Pages 1081–1268

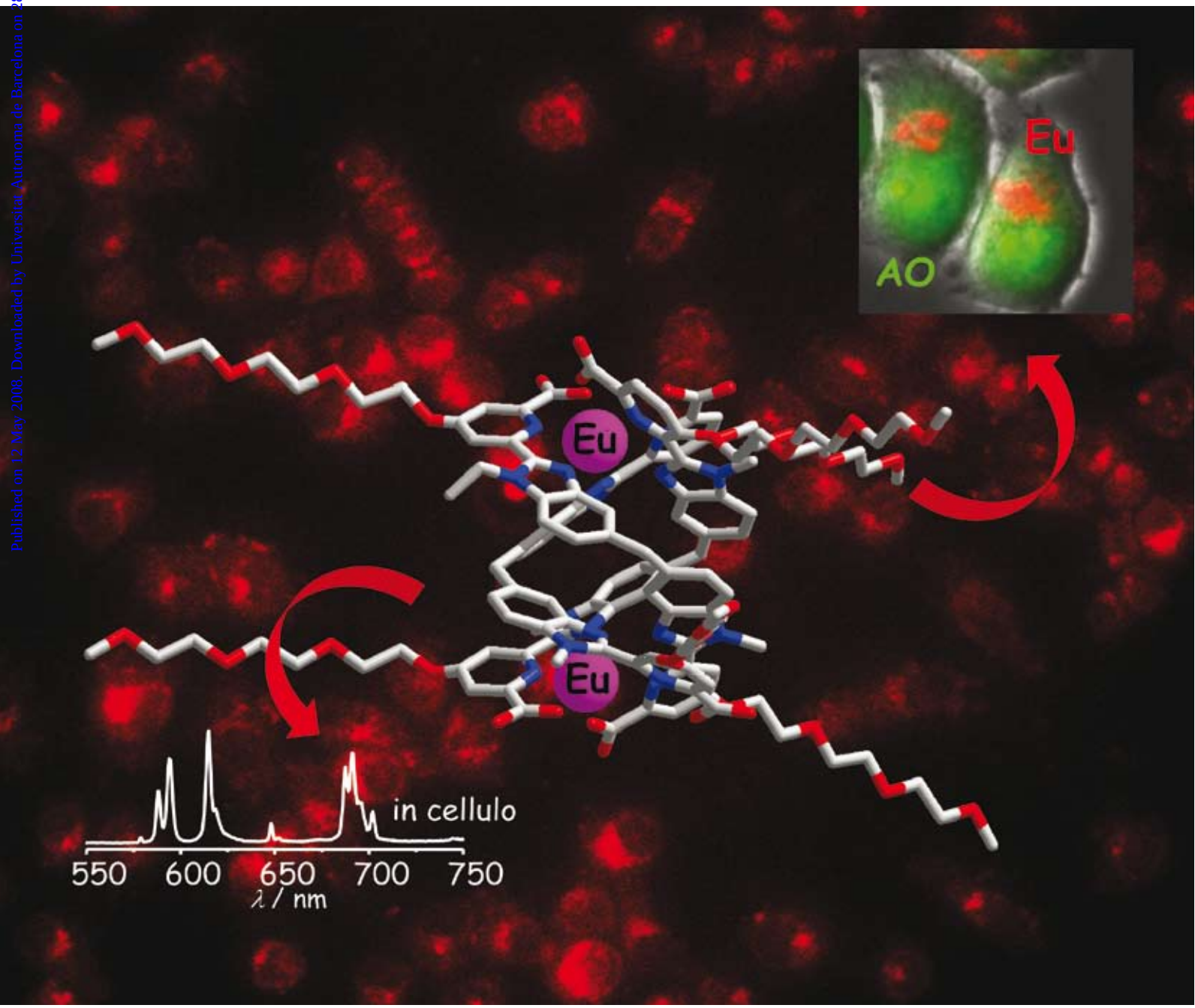

ISSN 1144-0546

RSC Publishing

CNRS CENTRE NATIONAL DE LA RECHERCHE SCIENTIFIQUE

PAPER

Jean-Claude Bünzli *et al.*

Effect of the length of polyoxyethylene substituents on luminescent bimetallic lanthanide bioprobes

Effect of the length of polyoxyethylene substituents on luminescent bimetallic lanthanide bioprobes†

Emmanuel Deiters, Bo Song, Anne-Sophie Chauvin, Caroline D. B. Vandevyver and Jean-Claude G. Bünzli

Received (in Montpellier, France) 11th January 2008, Accepted 13th March 2008
First published as an Advance Article on the web 12th May 2008
DOI: 10.1039/b800516h

The new homoditopic ligand $H_2L^{C2'}$ self-assembles with lanthanide ions (Ln^{III}) to yield neutral bimetallic helicates of overall composition $[Ln_2(L^{C2'})_3]$; it is fitted with two hexakis(oxyethylene) chains to test their effects on the thermodynamic, photophysical and biochemical properties of these complexes, with particular emphasis on their uptake by living cells. At physiological pH and under stoichiometric conditions, the conditional stability constants $\log \beta_{23}$ are around 28 resulting in the speciation of the Eu^{III} helicate being >92% for a total ligand concentration of 1 mM. The ligand triplet state features adequate energy (0-phonon transition at $\approx$21 800 cm^{-1}) for sensitising the luminescence of Eu^{III} (Q = 19%) and Tb^{III} (Q = 10%) in aerated water at pH 7.4. The $Eu(^5D_0)$ emission spectrum and lifetime (2.43 ms) are characteristic of a species with pseudo-D_3 symmetry and without bound water in the inner coordination sphere. The viability of HeLa cancerous cells is unaffected when incubated with up to 500 μM $[Eu_2(L^{C2'})_3]$ during 24 h. The Eu^{III} helicate permeates into the cytoplasm of these cells by endocytosis and remains essentially undissociated, despite a low intracellular concentration of 0.28 μM. In addition, the leakage of the Eu^{III} helicate out of HeLa cells is very minimal over long periods of time. With respect to similar complexes with ligands bearing shorter tris(oxyethylene) chains, no substantial changes are observed, which opens the way for targeting experiments. This study also demonstrates that the $[Ln_2(L^{CX})_3]$ helicates are fairly robust entities since their core is unaffected by the substitution in the pyridine 4-position.

Introduction

As the need for biolabels increases, both for tracking *in cellulo* processes,[1,2] elucidating receptor–ligand interactions,[3] mapping specific analytes,[4,5] developing high-throughput screening,[6] or imaging cells and organs,[7] trivalent lanthanide ions Ln^{III} are emerging as highly versatile luminescent centres for these purposes. Indeed, their distinctive spectroscopic properties,[8,9] in particular their high tolerance to photobleaching and the long lifetimes of their excited states allowing time-resolved detection, which eliminates unwanted background signals and autofluorescence, are real advantages over organic luminescent bioprobes.[10,11] This is already properly established for luminescence immunoassays[12] and the use of lanthanide ions in bio-active probes for medical diagnosis[13] or analyses[14] is well documented. The capacity of some luminescent lanthanide ions to emit in the near-infrared range is another advantage[14,15] in view of the transparency of biological tissues in this spectral range.[16] Until recently however, cell imaging experiments taking advantage of Ln^{III} luminescence have remained relatively scarce.[11,17–21]

We are presently developing a strategy aiming at incorporating two lanthanide ions in a single molecular triple-stranded helical structure[22] by thermodynamically controlled self-assembly of hexadentate, ditopic ligands with lanthanide ions.[23] There are several benefits linked to this strategy: (i) both homo- and hetero-bimetallic helicates can be assembled, opening the way for double-lanthanide tags containing either two emissive ions[24] or one emissive and one magnetic metal centres,[25,26] (ii) the self-assembly process operates at room temperature and is kinetically fast,[27,28] (iii) the ligands can be derivatised to incorporate coupling groups for biological targeting, and (iv) the helicates are intrinsically chiral so that adequate substitution should enable the isolation of a specific isomer, as has been done for 3d–4f assemblies,[29] or more recently for triple- and quadruple-stranded 4f–4f helicates with chiral bis(β-diketonates).[30]

The ligand design is based on bis(benzimidazole)pyridine tridentate units which induce nine-coordinate, tricapped trigonal prismatic environments around the 4f ions similar to those found in aqua ions (Scheme 1).[32,33] Such a molecular platform is versatile enough to allow the synthesis of (i) unsymmetrical ligands tailored for the recognition of a heteropair of metal ions, 4f–4f′[34–37] or 4f–3d ions,[26,38] with the aim of developing heterometallic bimodal probes, and (ii) of symmetrical ligands for inserting a homopair of lanthanide ions into a helical edifice. A viable luminescent bioprobe has to meet several stringent requirements, among them adequate

Laboratory of Lanthanide Supramolecular Chemistry, École Polytechnique Fédérale de Lausanne, BCH 1402, CH-1015 Lausanne, Switzerland. E-mail: jean-claude.bunzli@epfl.ch; Fax: +41 21 693 9825; Tel: +41 21 693 9821

† Electronic supplementary information (ESI) available: Figs. S1–S15: Additional characterization data. See DOI: 10.1039/b800516h

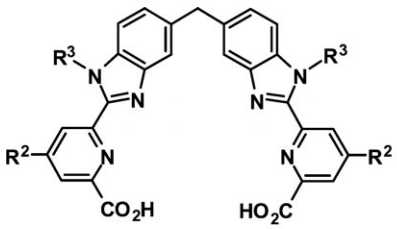

R^2	R^3	L
H	Et	H_2L^C
$(OCH_2CH_2)_3OMe$	Me	H_2L^{C2}
$(OCH_2CH_2)_6OMe$	Me	$H_2L^{C2'}$
H	$(CH_2CH_2O)_3Me$	H_2L^{C3}

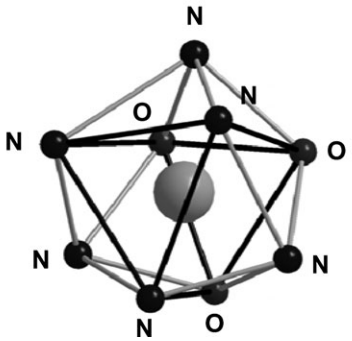

Scheme 1 (Top) Ditopic hexadentate ligands for the self-assembly of water-soluble triple-stranded homobimetallic helicates. (Bottom) Tricapped trigonal prismatic environment of Tb^{III} ions revealed by the X-ray crystal structure of $[Tb_2(L^C)_3]$ (redrawn from ref. 31).

photophysical properties, thermodynamic stability and kinetic inertness at physiological pH, and non-cytotoxicity. It also has to be water-soluble, so that our recent work has concentrated on derivatizing the dicarboxylic acid ligand H_2L^C,[31,39] (Scheme 1) which yields very stable neutral homobimetallic $[Ln_2(L^C)_3]$ helicates in water. The Eu^{III} luminescence is efficiently sensitized (quantum yield = 24%, $Eu(^5D_0)$ lifetime = 2.43 ms)[40] and the corresponding helicate shows no cytotoxicity.[41] On the other hand, extensive back transfer occurs for the Tb^{III} chelate, which is therefore inappropriate as bioprobe; moreover, the water solubility of these helicates is limited, particularly at pH < 4.[27] Introduction of a short polyoxyethylene side chain either on the 4-position of the pyridines (H_2L^{C2})[42,43] or on the benzimidazoles (H_2L^{C3})[40] results in much more soluble helicates, which are also non-cytotoxic. They are internalized into several cancerous cell lines by endocytosis and stain their cytoplasm. When comparing the chemical stability, cell imaging properties, and derivatization potential for targeting purposes, helicates with H_2L^{C2} appear to be best suited as bioprobes, particularly that the back transfer problem for Tb^{III} is almost eliminated.[43]

We address here the question of whether or not the length of the polyoxyethylene substituent in R^2 influences the specific properties of the helicates, particularly their uptake into living HeLa cells in view of their enhanced hydrophilicity when the number of (OCH_2CH_2) units is increased from three to six. Indeed, a recent paper has demonstrated that the replacement of *N*-carboxymethyl by longer *N*-carboxyethyl pendant arms in $^{64}Cu^{II}$ complexes with cyclam derivatives significantly improves the biological behaviour of the corresponding radiopharmaceuticals.[44] Finally, longer substituents in addition to help avoiding the stacking of the luminescent bioprobes in living cells are also interesting for coupling experiments requiring some distance between the luminescent stain and the targeted site, for instance to avoid quenching of the metal-centred luminescence by the biological target.

Experimental

Starting materials and analytical procedures

Chemicals and solvents were purchased from Fluka A. G. and Aldrich. Solvents were purified by a non-hazardous procedure by passing them onto activated alumina columns (Innovative Technology Inc. system).[45] ^1H NMR spectra of the reaction intermediates were acquired on a Bruker Avance DRX 400 spectrometer (400 MHz) and ^{13}C NMR spectra on a Bruker AV 600 (600 MHz) at 25 °C with deuterated solvents as internal standards; chemical shift values are given in ppm with respect to TMS and *J* values are reported in Hz. The ligand spectra were measured on a Bruker AV 800 (800 MHz) spectrometer. ESI-MS spectra were obtained with a Finnigan SSQ 710C spectrometer using 10^{-5}–10^{-4} M solutions in acetonitrile–H_2O–acetic acid (50 : 50 : 1) or MeOH; the capillary temperature was set to 200 °C, the acceleration potential to 4.5 keV, and the ion spray voltage to 4.6 kV. The instrument was calibrated with horse myoglobin and analyses were conducted in positive mode. ESI-TOF spectra in positive ion mode were recorded on a Q-TOF Ultima mass spectrometer (Micromass, Manchester, UK) equipped with a Z-spray type ESI source. Phosphoric acid was used for mass calibration in the range 100–2000 m/z. Data were acquired and processed with Masslynx version 4.0. Electrospray conditions were as follows: capillary voltage, 3 kV; source temperature, 80 °C; cone voltage, 35 V; source block temperature, 150 °C. The ESI nebulisation and drying gas was nitrogen. The sample was introduced *via* a syringe pump operating at 20 μl min^{-1}. Elemental analyses were performed by Dr Eder, Microchemical Laboratory of the University of Geneva or by Dr E. Solari from the Elemental Analysis Laboratory of ISIC, EPFL.

Synthesis of the ligand (Scheme 2)

4-Hydroxypyridine-2,6-dicarboxylic acid diethyl ester (**2**) was synthesized as previously described.[43]

Hexaethylene glycol monomethyl ether (3)

Hexaethylene glycol (515 mg, 1.77 mmol) and NaOH (117 mg, 2.92 mmol) were introduced into a two-necked round bottomed flask under vigorous stirring. This mixture was warmed to approximately 120 °C until complete dissolution of the solid. The temperature was then decreased to 80 °C and Me_2SO_4 (766 mg, 1.77 mmol) was added dropwise. This temperature was maintained for 4 h. After cooling to rt, distilled water (10 ml) was added and the aqueous phase was extracted with CH_2Cl_2 (5 × 30 ml). The organic phases were combined, dried over Na_2SO_4, filtered and evaporated to dryness. The resulting crude product was purified by column

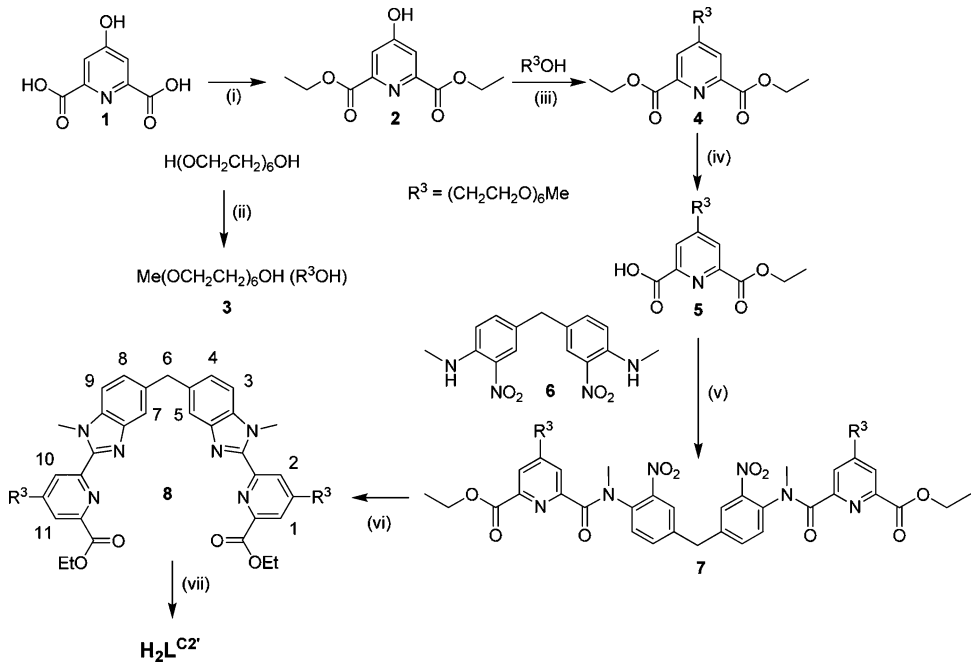

Scheme 2 Synthesis of the ditopic ligand $H_2L^{C2\prime}$ with the atom-numbering scheme used for discussing NMR spectra showed for **8**. *Reagents and conditions*: (i) H_2SO_4, EtOH, reflux (4 h); (ii) NaOH, 120 °C then Me_2SO_4, 80 °C (4 h); (iii) DIAD, Ph_3P, THF, reflux (12 h); (iv) NaOH, H_2O, rt (1 h); (v) $SOCl_2$, CH_2Cl_2, DMF, reflux (2 h) then 6, NEt_3, CH_2Cl_2, reflux (12 h); (vi) Fe, EtOH, H_2O, HCl, reflux (12 h) then EtOH, H_2SO_4, reflux (12 h); (vii) NaOH, EtOH, 60 °C (1 h).

chromatography (silica gel, CH_3CN–MeOH, 100 : 0 → 95 : 5) to give an amber oil (210 mg, 40%). Anal. Calc. for $C_{13}H_{28}O_7$: C, 52.68; H, 9.52. Found: C, 52.47; H, 9.51%. ^{1}H NMR ($CDCl_3$): δ 3.73 (m, 2H, CH_2OH), 3.60–3.69 (m, 20 H), 3.54 (m, 2H, CH_2OCH$_3$), 3.37 (s, 3H, OCH$_3$). ^{13}C NMR ($CDCl_3$): δ 72.49 (*C*H$_2$CH$_2$OH), 71.94 (CH$_2$*C*H$_2$OCH$_3$), 70.97 (CH$_2$O), 70.57 (CH$_2$O), 70.52 (CH$_2$O), 70.27 (*C*H$_2$CH$_2$OCH$_3$), 61.68 (CH$_2$*C*H$_2$OH), 59.01 (OCH$_3$). ESI-MS: *m*/*z* 297.33 ([M + H$^+$], calc.: 297.19).

4-{2-[2-(2-Methoxyethoxy)ethoxy]4-ethoxy}pyridine-2,6-dicarboxylic acid diethyl ester (4)

4-Hydroxypyridine-2,6-dicarboxylic acid diethyl ester (1.35 g, 5.84 mmol), hexaethylene glycol monomethyl ether (2.60 g, 8.77 mmol) and triphenyl phosphine (2.30 g, 8.77 mmol) were dissolved in THF (50 ml). DIAD (1.89 g, 8.77 mmol) was then slowly added under stirring (slightly exothermic) and the solution was refluxed overnight. The solvent was evaporated and dried under vacuum. The residue was then charged on a column chromatography (silica gel, AcOEt–MeOH, 100 : 0 → 90 : 10) to provide the desired product as a colourless oil (2.06 g, 68%). ^{1}H NMR ($CDCl_3$): δ 7.80 (s, 2H, H$_{3,5\text{-Py}}$), 4.46 (q, 4H, ^3J = 7.2, OCH_2CH$_3$), 4.30 (t, 2H, ^3J = 4.6, CH_2CH$_2$O-Py), 3.90 (t, 2H, ^3J = 4.6, CH_2CH$_2$OPy), 3.71 (m, 2H, CH_2CH$_2$OCH$_3$), 3.61–3.68 (m, 16H, (CH$_2$CH$_2$O)$_4$), 3.54 (m, 2H, CH$_2$CH_2OCH$_3$), 3.37 (s, 3H, OCH$_3$), 1.44 (t, 6H, ^3J = 7.2, OCH$_2$CH_3). ^{13}C NMR ($CDCl_3$): δ 166.18 (C$_{\text{Py–O quat.}}$), 164.69 (C=O), 150.16 (C$_{\text{Py, quat.}}$), 114.44 (C$_{\text{Py.}}$), 71.95 (PyOCH$_2$), 71.01 (OCH$_2$), 70.79 (OCH$_2$), 70.62 (OCH$_2$), 69.16 (OCH$_2$), 62.41 (OCH$_2$CH$_3$), 57.22 (OCH$_3$), 14.21 (OCH$_2$CH$_3$). ESI-MS: *m*/*z* 518.36 ([M + H$^+$], calc.: 518.26).

4-{2-[2-(2-Methoxyethoxy)ethoxy]4-ethoxy}pyridine-2,6-dicarboxylic acid monoethyl ester (5)

An amount of **4** (2.06 g, 4.21 mmol) was dissolved in 3 ml of an aqueous NaOH solution (85 mg, 2.11 mmol) and the mixture was vigorously stirred for 1 h at rt. Disappearance of the starting material was checked by TLC (silica sheet, AcOEt–MeOH 95 : 5 v/v). Distilled water (20 ml) was then added and the resulting basic solution was extracted with CH_2Cl_2 (5 × 200 ml). The aqueous fraction was acidified until pH 2 by addition of HCl 0.1 M and extracted with CH_2Cl_2 (5 × 200 ml), dried over Na_2SO_4 and evaporated. The overall procedure was repeated three more times to obtain **5** as a pale yellowish oil (0.99 g, 51%). ^{1}H NMR ($CDCl_3$): δ 7.87 (d, 1H, ^4J = 2.2, H$_{\text{Py}}$), 7.85 (d, 1H, ^4J = 2.2, H$_{\text{Py}}$), 4.46 (q, 2H, ^3J = 7.0, OCH_2CH$_3$), 4.33 (t, 2H, ^3J = 4.3, CH$_2$CH_2OPy), 3.91 (t, 2H, ^3J = 4.3, CH_2CH$_2$OPy), 3.72 (t, 2H, ^3J = 5.0, CH_2CH$_2$OCH$_3$), 3.62–3.67 (m, 16H, (CH$_2$CH$_2$O)$_4$), 3.53 (t, 2H, ^3J = 5.0, CH$_2$CH_2OCH$_3$), 3.35 (s, 3H, OCH$_3$), 1.43 (t, 3H, ^3J = 7.0, OCH$_2$CH_3). ^{13}C NMR ($CDCl_3$): δ 167.91 (C$_{\text{Py–O quat.}}$), 163.65 (C=O), 163.56 (C=O), 148.43 (C$_{\text{Py, quat.}}$), 148.14 (C$_{\text{Py. quat.}}$), 116.07 (C$_{\text{Py}}$), 111.99 (C$_{\text{Py}}$), 71.91 (PyOCH$_2$), 70.97 (OCH$_2$), 70.63 (OCH$_2$), 70.61 (OCH$_2$), 70.58 (OCH$_2$), 70.56 (OCH$_2$), 70.54 (OCH$_2$), 70.53 (OCH$_2$), 70.48 (OCH$_2$), 69.07 (OCH$_2$), 68.71 (OCH$_2$), 62.36 (OCH$_2$CH$_3$), 59.00 (OCH$_3$), 14.20 (OCH$_2$CH$_3$). ESI-MS: *m*/*z* 490.34 ([M + H$^+$], calc.: 490.23).

Compounds 7 and 8

A mixture of **5** (765 mg, 1.65 mmol), freshly distilled $SOCl_2$ (1.86 g, 15.6 mmol), and dry DMF (12 ml, 0.156 mmol) were refluxed for 120 min in dry CH_2Cl_2 (50 ml) under an inert

atmosphere. After evaporation and pumping for 2 h, the pale yellow oil formed was redissolved in dry CH_2Cl_2 (50 ml) and NEt_3 (2 ml). 3,3′-Dinitro-4,4′-bis(*N*-methylamino)diphenylmethane **6**, synthesized by a known procedure[46] (190 mg, 0.601 mmol) and dissolved in 25 ml of dry CH_2Cl_2, was added dropwise to this solution which was then refluxed under an inert atmosphere for 12 h and evaporated. The brown residue was redissolved in CH_2Cl_2 (100 ml) and washed with a half-saturated NH_4Cl solution (2 × 100 ml). The combined organic phases were dried over Na_2SO_4, evaporated, and the resulting crude solid was purified by column chromatography (silica gel; CH_2Cl_2–MeOH, 100 : 0 → 93 : 7 v/v) to give the disubstituted product **7** as an orange oil (756 mg, 93%). This somewhat unstable product was directly converted into **8** without further purification. ESI-MS: *m*/*z* 1259.81 ([M + H^+], calc.: 1259.55), 630.35 ([M + 2H^+]/2, calc.: 631.27), 1281.30 ([M + Na^+], calc.: 1281.53).

Freshly activated iron powder (0.94 g, 16.7 mmol) and HCl (4.4 ml, 37%) were added to an ethanol–water solution (118 : 33 ml) containing **7** (700 mg, 0.556 mmol). The mixture was refluxed overnight under an inert atmosphere. The solution was cooled, the excess of unreacted iron filtered off, and the solvents were evaporated. The crude product was redissolved in absolute EtOH (40 ml). Sulfuric acid (2 ml, 97%) was added carefully, the solution was refluxed overnight, cooled, and the solvents were removed. Distilled water (100 ml) was added and the pH was adjusted to 6 with a saturated solution of aqueous $NaHCO_3$; Na_2H_2EDTA (4.14 g, 11.1 mmol) was then added to this solution, prior to the addition of a H_2O_2 solution (1 ml, 30%); the colour of the mixture turned to brown. ***CAUTION!*** *Hydrogen peroxide combined with organic compounds is potentially explosive and should be handled in small quantities and with adequate precautions*. The pH was then increased to 7 with a saturated solution of aqueous $NaHCO_3$ before extraction with CH_2Cl_2 (2 × 500 ml). This extraction procedure was repeated two more times. Then the organic phases were combined and extracted again with a saturated solution of aqueous $NaHCO_3$ containing Na_2H_2EDTA (4.14 g), dried over Na_2SO_4, filtered, and evaporated to dryness, resulting in a brown crude solid which was purified by column chromatography (silica gel; CH_2Cl_2–MeOH, 100 : 0 → 95 : 5) to give a pale orange solid (200 mg, 31%). ^{1}H NMR ($CDCl_3$): δ 8.08 (d, 2H, ^4J = 2.3, H_{Py}), 7.69 (d, 2H, ^4J = 2.3, H_{Py}), 7.67 (s, 2H, $H_{Benz.}$), 7.33 (d, 2H, ^3J = 8.3, $H_{Benz.}$), 7.24 (d, 2H, ^3J = 8.3, H_{Benz}), 4.45 (q, 4H, ^3J = 7.0, OCH_2CH_3), 4.35 (s, 6H, NCH_3), 4.33 (t, 4H, ^3J = 4.3, CH_2CH_2OPy), 4.26 (s, 2H, CH_2), 3.90 (t, 4H, ^3J = 4.3, CH_2CH_2OPy), 3.72 (m, 4H, $CH_2CH_2OCH_3$), 3.60–3.68 (m, 36H, $(CH_2CH_2O)_4$), 3.52 (m, 4H, $CH_2CH_2OCH_3$), 3.35 (s, 6H, OCH_3), 1.44 (t, 6H, ^3J = 4.3, OCH_2CH_3). ^{13}C NMR ($CDCl_3$): δ 166.33 ($C_{Py–O\ quat.}$), 164.90 (C═O), 152.32 ($C_{Benz,\ quat.}$), 149.29 ($C_{Py.\ quat.}$), 148.60 ($C_{Py.\ quat.}$), 142.62 ($C_{Py.\ quat.}$), 136.50 ($C_{Py.\ quat.}$), 136.08 ($C_{Py.\ quat.}$), 125.10 ($C_{Benz.}$), 119.88 ($C_{Benz.}$), 113.34 ($C_{Py.}$), 111.75 ($C_{Benz.}$), 109.99 ($C_{Py.}$), 71.90 ($PyOCH_2$), 70.94 (OCH_2), 70.63 (OCH_2), 70.61 (OCH_2), 70.58 (OCH_2), 70.56 (OCH_2), 70.55 (OCH_2), 70.53 (OCH_2), 70.49 (OCH_2), 69.19 (OCH_2), 68.20 (OCH_2), 61.83 (OCH_2CH_3), 59.02 (OCH_3), 42.25 (–CH_2–), 32.95 (NCH_3), 14.26 (OCH_2CH_3). ESI-MS: *m*/*z* 1163.84 ([M + H^+], calc.: 1163.58), 582.83 ([M + 2H^+]/2, calc.: 583.28).

Ligand $L^{C2'}$

An amount of **8** (200 mg, 0.172 mmol) was dissolved in absolute EtOH (25 ml) containing NaOH (28 mg, 0.688 mmol). This mixture was heated at 60 °C for 2 h. After completion of the reaction, the basic aqueous solution was washed with CH_2Cl_2 (5 × 200 ml), then it was acidified to pH 2.0 by addition of HCl 0.02 M. The latter solution was extracted with CH_2Cl_2 (5 × 200 ml), dried over Na_2SO_4, and evaporated to give a pale brown solid. This crude product was subsequently purified by column chromatography (silica gel; CH_3CN–NH_3(aq), 100 : 0 → 80 : 20) to give a pale yellow solid (68 mg, 36%). Anal. Calc. for $C_{55}H_{72}N_6O_{18}$·0.75NaCl·NH_4OH: C, 55.74; H, 6.55; N, 8.27. Found: C, 55.97; H, 6.51; N, 8.11%. ^{1}H NMR (800 MHz, CD_3OD): δ 8.09 (d, 2H, ^4J = 2.2, H_{Py}), 7.92 (d, 2H, ^4J = 2.2, H_{Py}), 7.59 (s, 2H, H_{Benz}), 7.54 (d, 2H, ^3J = 8.6, H_{Benz}), 7.33 (d, 2H, ^3J = 8.6, H_{Benz}), 4.40 (t, 4H, ^3J = 4.8, CH_2CH_2OPy), 4.27 (s, 6H, ^3J = 4.8, NCH_3), 4.27 (s, 2H, CH_2), 3.93 (m, 4H, CH_2CH_2OPy), 3.47–3.71 (m, 36H, CH_2 chain), 3.41 (m, 4H, $CH_2CH_2OCH_3$), 3.31 (s, 6H, OCH_3). ^{13}C NMR (800 MHz, CD_3OD): δ 168.23 (C═O), 167.79 ($C_{Py–O\ quat.}$), 151.89 ($C_{Benz.\ quat.}$), 151.54 ($C_{Py.\ quat.}$), 151.02 ($C_{Py.\ quat.}$), 142.91 ($C_{Benz.\ quat.}$), 138.87 ($C_{Benz.\ quat.}$), 136.76 ($C_{Benz.\ quat.}$), 126.79 ($C_{Benz.}$), 118.92 ($C_{Benz.}$), 114.09 ($C_{Py.}$), 113.79 ($C_{Py.}$), 111.79 ($C_{Benz.}$), 72.90 ($PyOCH_2$), 71.85 (OCH_2), 71.58 (OCH_2), 71.51 (OCH_2), 71.49 (OCH_2), 71.45 (OCH_2), 71.27 (OCH_2), 70.39 (OCH_2), 69.64 (OCH_2), 59.07 (OCH_3), 42.91 (–CH_2–), 33.05 (NCH_3). ESI-MS: *m*/*z* 1107.38 ([M + H^+], calc.: 1107.51, 554.29 (M + 2H^+]/2, calc.: 554.26).

Preparation of the lanthanide salts

Stock solutions of lanthanides were prepared prior their use in doubly distilled water from the corresponding $Ln(ClO_4)_3$·xH_2O salts (Ln = La, Lu, Gd, Tb, Eu, x = 2.5–4.5). These salts were obtained from their oxides (Rhône-Poulenc, 99.99%) in the usual way.[47] Concentrations of the solutions were determined by complexometric titrations with a standardized Na_2H_2EDTA solution in urotropine buffered medium and with xylenol orange as indicator.[48] ***CAUTION!*** *Perchlorate salts combined with organic ligands are potentially explosive and should be handled in small quantities and with adequate precautions*.[49]

Physico-chemical measurements

UV-Visible spectra were measured in 0.2-cm quartz Suprasil® cuvettes on a Perkin Elmer Lambda 900 spectrometer. Protonation constants of $H_2L^{C2'}$ were determined with the help of a J&M diode array spectrometer (Tidas series) connected to an external computer. All titrations were performed in a thermostated (25.0 ± 0.1 °C) glass-jacketed vessel at μ = 0.1 M (KCl). Stability constants were determined by titration of $H_2L^{C2'}$ with Ln^{III} (Ln = La, Eu, Lu) at fixed pH 7.4 (0.1 M Tris-HCl buffer). Factor analysis[50] and mathematical treatment of the spectrophotometric data were performed with the Specfit® software.[51]

Potentiometric titration of $(H_6L^{C2'})^{4+}$ achieved on a 5 ml sample 1.022 × 10^{-3} M in H_2O in a thermostated (25.0 ± 0.1 °C) glass-jacketed vessel under an Ar atmosphere.

The ionic strength was fixed with KCl (μ = 0.1 M). The solution was acidified to a pH of ~1.7 with fuming HCl 30 min before titration. Titrations were carried out with an automatic Metrohm Titrino 736 GP potentiometer linked to an IBM PS/2 computer (resolution 0.1 mV, accuracy 0.2 mV) using constant volume addition (0.0125 ml). An automatic burette (Metrohm 6.3013.210, 10 ml, accuracy 0.03 ml) was used along with a Metrohm 6.0228.000 glass electrode. The standard base solution (0.1 M NaOH) was added inside the solution through a capillary tip attached to the automatic burette. The data (200 points, drift <1 mV/min) were mathematically treated by the program HYPERQUAD2000 using a Marquardt algorithm. Calibration of the pH meter and the electrode system was performed prior to each measurement using a standardized 0.1 M NaOH solution, and the electrode readings were converted to pH.

Luminescence spectra and lifetimes were collected either on a Horiba-Jobin Yvon Fluorolog FL 3-22 fluorimeter or on a home-made high-resolution set-up, according to procedures published previously.[40,52] When bi-exponential analysis of the luminescence decay was required, the populations of the corresponding species were calculated according to:

$$\%A_1 = \frac{A_1\tau_1}{A_1\tau_1 + A_2\tau_2} \times 100 \qquad (1)$$

where A_1 and A_2 are the intensity factors of the individual exponential functions and τ_1 and τ_2 the corresponding lifetimes. Emission and excitation spectra are corrected for the instrumental function, which has been regularly updated.

Quantum yields were measured both by a comparative method with $[Eu_2(L^C)_3]$ as standard (Q = 24%)[40] and by an absolute method using an integration sphere.[43,53] The obtained data are averages of at least three determinations and are within the accuracy limits of the methods, estimated to ±10%, as shown in Table 1.

Cell imaging experiments and analyses

Cell lines. The human cervical adenocarcinoma cell line HeLa (ATCC CCL-2) was used in this study. Cells were cultivated in 75 cm^2 culture flasks using RPMI-1640 supplemented with 5% foetal calf serum (FCS), 2 mM L-glutamine, 1 mM sodium pyruvate, 1% non-essential amino-acids, 1% 4-(2-hydroxyethyl)monosodium salt (HEPES) (all from Gibco® Cell Culture, Invitrogen, Basel, Switzerland). Cultures were maintained at 37 °C under 5% CO_2 and 95% air atmosphere. The growth medium was changed every other day until the time of use of the cells. Cell density and viability, defined as the ratio of the number of viable cells over the total number of cells, of the cultures were determined by Trypan Blue staining and a Neubauer improved hemacytometer (Blau Brand, Wertheim, Germany).

Table 1 Quantum yields of the $[Ln_2(L^{C2\prime})_3]$ helicates determined in Tris-HCl buffer (0.1 M in H_2O) by two different methods

Compound	c/μM	λ_{exc}/nm	$A_x(\lambda_{exc.})^a$ or $(1-T)^b$ (%)	$Q \pm 2\sigma$ (%)
$[Eu_2(L^C)_3]$	16.6	332	0.1972	24.0[c]
$[Eu_2(L^{C2\prime})_3]$	12.1	321	0.1817	19.8 ± 0.7[d]
	15.0	321	34.8	18.5 ± 1.0[e]
$[Tb_2(L^{C2\prime})_3]$	11.4	321	0.1817	10.9 ± 0.3[d]
	15.0	321	44.0	9.7 ± 0.1[e]

[a] Absorbance (comparative method). [b] T is the transmission (absolute method). [c] From ref. 43. [d] Comparative method. [e] Absolute method.

WST-1 cell proliferation assay. This assay is dependent on the cellular reduction of the WST-1 cell proliferation reagent, (4-(3-(4-iodophenyl)-2-(4-nitrophenyl)-2*H*-5-tetrazolio)-1,3-benzene disulfonate (Roche, Germany) by mitochondrial dehydrogenases in viable cells, which leads to a dark red formazan product. The viable cell number per well is directly proportional to the production of formazan, which can be measured spectrophotometrically.[54,55] Cells were seeded in a 96-well tissue culture microplate at a concentration between 1–5 × 10^5 cells $well^{-1}$ in 100 μl culture medium and incubated overnight at 37 °C and 5% CO_2. The Eu^{III} helicate was dissolved in fresh RPMI-1640 medium at 37 °C, at a concentration of 500 μM. The medium was removed from the cell cultures and 100 μl $well^{-1}$ of the chelate was added (final concentrations: 500, 250 and 125 μM); 10 μl of WST-1 reagent were added to each well and the plate was shaken for 1 min on a microtiter plate shaker (450 rpm). The plate was further incubated at 37 °C and 5% CO_2 and the absorbance of the formazan product was measured at 450 nm with an ELISA reader (Spectra MAX 340, Molecular Devices, Sunnyvale, CA, USA). Cell viability was calculated from the absorbance values as:

$$\text{viability}_{WST}[\%] = \frac{(A_{450} - A_{650})_{exp}}{(A_{450} - A_{650})_{medium}} \times 100 \qquad (2)$$

where $A_{450} - A_{650}$ is the absorbance difference between 450 nm and 650 nm for the cells that were in contact with the complex ("exp") and the medium. The results are expressed as an average over three nominally identical measurements.

Live cell imaging. For luminescence microscopy, cells were seeded on glass bottom cell culture dishes and loaded with the complex dissolved in freshly prepared cell culture medium. The incubation time varied from 15 min to 24 h, and the concentration of the added complex was in the range of 5 to 500 μM. Cells were incubated at 37 or 4 °C for the indicated time and washed at least six times with phosphate buffer saline (PBS) before examination under the microscope.

Quantitation of the intracellular concentration of $[Eu_2(L^{C2\prime})_3]$ using Delfia® assays. All incubations for the Delfia® assays were carried out at rt with stirring in a final volume of 200 μl. HeLa cells were cultivated in 6-well cell culture plates and loaded overnight with 25 μM $[Eu_2(L^{C2\prime})_3]$ dissolved in fresh cell culture medium at 37 °C. The cells were washed with PBS at least 10 times and harvested by trypsin treatment. The number of labelled cells suspended in a known volume of PBS was counted by Trypan Blue staining and a Neubauer improved hemacytometer (Blau Brand, Wertheim, Germany). Cells were seeded at 50, 500 and 1000 cells/100 μl in a 96-well Delfia® plate and 100 μl Delfia®. Inducer was added to induce complete cell lysis. The plate was shaken vigorously for 5 min and was read in 1234 Delfia® fluorometer plate reader (Perkin

Elmer Life and Analytical Sciences) using an europium protocol (excitation at 320 nm, emission at 615 nm, delay 400 μs, 1 ms integration time/cycle). To generate a standard curve, a known number of cells in 100 μl were spiked with 1 μM to 1 pM [$Eu_2(L^{C2'})_3$], 100 μl Delfia® Inducer was added, and the Eu luminescence was measured as above. Each point of the calibration curve is the average of four nominally identical measurements.

***In cellulo* photophysical data.** HeLa cells at 90% confluency were loaded overnight with the helicate (250 μM in RPMI-1640 culture medium), washed with PBS ten times, and then harvested with trypsin. The mixture was centrifuged (2000 tr min^{-1}, 4 min), and the cell pellet was re-suspended in PBS (0.8 ml). The emission spectrum of the Eu^{III} helicate localized in cells was then recorded on the Fluorolog spectrometer.

Results and discussion

Synthesis and protonation constants of the ligand

The hexadentate ligand $H_2L^{C2'}$ was synthesized following the reaction path described on Scheme 2. As for H_2L^{C2}, the hexakis(oxyethylene) substituents were introduced at an early stage of the synthesis *via* a Mitsunobu reaction. Modified double Phillips coupling reaction[56] led to the formation of the benzimidazole rings in **8**, followed by hydrolysis to produce the final compound. Ligand deprotonation constants were determined at 25 °C by spectrophotometric and potentiometric titrations of $H_2L^{C2'}$ with sodium hydroxide at constant ionic strength (0.1 M KCl) and in the pH range 1.11–12.86. The absorption spectra display two major isosbestic points at 240 and 320 nm (Fig. S1, top, ESI†). Factor analysis yields seven absorbing species, but the best fit of data corresponds to the following set of equations taking into account six species only (the first number is from spectrophotometric titration, the second from potentiometric measurements):

$$(H_6L^{C2'})^{4+} \leftrightarrows (H_4L^{C2'})^{2+} + 2H^+ : (pK_{a1} + pK_{a2}) = 4.6(1)/4.5(1) \quad (3)$$

$$(H_4L^{C2'})^{2+} \leftrightarrows (H_3L^{C2'})^{+} + H^+ : pK_{a3} = 4.3(1)/4.1(1) \quad (4)$$

$$(H_3L^{C2'})^{+} \leftrightarrows (H_2L^{C2'}) + H^+ : pK_{a4} = 5.7(1)/5.8(1) \quad (5)$$

$$(H_2L^{C2'}) \leftrightarrows (HL^{C2'})^{-} + H^+ : pK_{a5} = 8.3(1)/8.2(1) \quad (6)$$

$$(HL^{C2'})^{-} \leftrightarrows (L^{C2'})^{2-} + H^+ : pK_{a6} = 10.7(1)/10.83(3) \quad (7)$$

The re-calculated spectra are shown on Fig. S1 (bottom, ESI†) while extractions at five different wavelengths of experimental and re-calculated spectra are in very good agreement (Fig. S2, ESI†), pointing to the consistency of the analysis. Generally speaking, the agreement between the pK_as extracted from spectrophotometric and potentiometric titrations is quite satisfying. As for ligands H_2L^{C2},[43] and H_2L^{C3},[40] only the sum of the first two pK_as could be determined and the assignment is similar: the two more acidic pK_as correspond to deprotonation of the carboxylic acid functions, the two middle pK_as to deprotonation of the pyridyl units, while the more basic ones refer to de-protonation of the imidazolium groups. Significant differences with respect to H_2L^{C2} occur only for pK_{a3} and pK_{a4} which are more acidic in our case by about one unit. There are also large deviations from the expected statistical differences, revealing the presence of intra- or inter-molecular interactions. For instance, strong hydrogen bonding can occur between the pyridinium proton and either the carboxylate or imidazolium groups, which may be substantially affected by the substituent on the para position of the pyridine ring. The distribution diagram computed from the fitted pK_as values is presented on Fig. S3 (ESI†): at physiological pH, neutral ($H_2L^{C2'}$) accounts for 87% of all the species in equilibrium.

Complex speciation in water at pH 7.4

The ^1H NMR spectrum of a stoichiometric solution of lanthanum perchlorate (6.4×10^{-4} M) and $H_2L^{C2'}$ (9.6×10^{-4}) M in D_2O displays a single set of reasonably sharp resonances for the three ligand strands (Fig. 1). This is in contrast with the spectrum of the un-complexed ligand which consists in broad and split signals owing to the presence of an equilibrium between at least two conformations exchanging slowly on the NMR time scale. The sharp and unique signals for the La^{III} solution point to the equivalence of the three ligand strands, reflecting the presence of one main species in solution, namely [$La_2(L^{C2'})_3$]. The aromatic protons are typical, with only two signals for the pyridine protons H1/H11 (6.05 ppm, see Scheme 2 for the atom numbering) and H2/H10 (6.98 ppm), which are shielded upon complexation. The benzenic protons H5/H7 (7.68 ppm) also give rise to a singlet while the expected doublets for H3/H9 and/or H4/H10 are seen at 7.23 and/or 7.41 ppm (^3J = 8.0 Hz). The bridging methylene protons H6 generate one (somewhat broadened) singlet which clearly indicates an A_2 spin system representative of two C_2-related enantiotopic protons. This is of importance since it means that the species in solution has pseudo-D_3 overall symmetry bringing additional proof for the complex being a triple-stranded bimetallic helicate with two equivalent metal-ion binding sites (compare also one singlet for all of the OMe groups at 3.28 ppm and one for the NMe groups at 4.06 ppm). That is, the grafting of the bulky polyoxyethylene substituent in the *para* position of the pyridine rings has little effect on the triple helical arrangement of the molecular core.

The species resulting from the interaction of trivalent lanthanide ions (Ln = La, Eu, Gd, Tb, and Lu) with $H_2L^{C2'}$

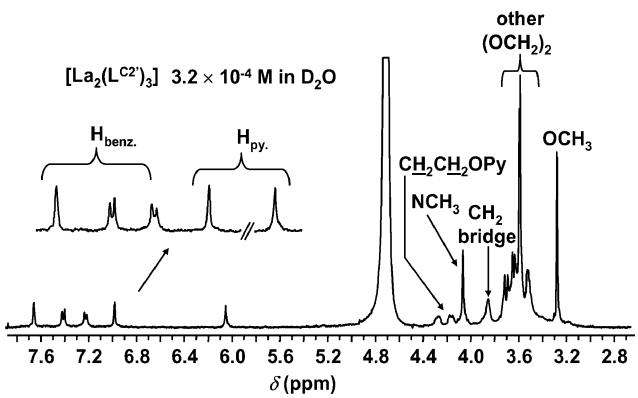

Fig. 1 ^1H NMR spectrum of a 2 : 3 stoichiometric solution of $La(ClO_4)_3 \cdot nH_2O$ and $H_2L^{C2'}$ ($c = 9.6 \times 10^{-4}$ M) recorded at room temperature in D_2O.

Table 2 Mass spectrometric data for $H_2L^{C2'}$ and stoichiometric 2 : 3 (Ln : $H_2L^{C2'}$) solutions in water–acetonitrile (90 : 10, v/v) with total ligand concentration 3.8×10^{-4} M

Species	Assignment	*m*/*z* (obs.)	*m*/*z* (calc.)	*M*[a]/Da
$(H_2L^{C2'})$	$[(H_2L^{C2'}) + Na^+]$	1129.37	1129.50	1106.50
	$[(H_2L^{C2'}) + Na^+]/2$	565.12	564.75	
$[La_2(L^{C2'})_3]$	$\{[La_2(L^{C2'})_3] + 3H^+\}/3$	1198.61	1198.80	3593.38
$[La_2(L^{C2'})_2]^{2+}$	$\{[La_2(L^{C2'})_2]^{2+}\}/2$	1243.89	1243.89	2486.79
$[Eu_2(L^{C2'})_3]$	$\{[Eu_2(L^{C2'})_3] + 3H^+\}/3$	1207.46	1207.44	3619.31
	$\{[Eu_2(L^{C2'})_3] + 4H^+\}/4$	905.91	905.83	
$[Eu_2(L^{C2'})_2]^{2+}$	$\{[Eu_2(L^{C2'})_2]^{2+} + K^+\}/4$	637.76	638.45	2514.82
	$\{[Eu_2(L^{C2'})_2]^{2+} + 2K^+\}/4$	648.27	648.18	
$[Gd_2(L^{C2'})_3]$	$\{[Gd_2(L^{C2'})_3] + 3H^+\}/3$	1210.63	1210.78	3629.32
$[Tb_2(L^{C2'})_3]$	$\{[Tb_2(L^{C2'})_3] + 3H^+\}/3$	1211.96	1211.11	3631.32
$[Tb_2(L^{C2'})_2]^{2+}$	$\{[Tb_2(L^{C2'})_2]^{2+}\}/2$	1264.24	1263.91	2526.83
$[Lu_2(L^{C2'})_3]$	$\{[Lu_2(L^{C2'})_3] + 3H^+\}/3$	1222.65	1222.84	3665.50
$[Lu_2(L^{C2'})_2]^{2+}$	$\{[Lu_2(L^{C2'})_2]^{2+}\}/2$	1279.73	1279.93	2560.31

[a] Molecular weight of the parent species.

3.8×10^{-4} M in water–acetonitrile (90 : 10) were further characterized by ESI-TOF mass spectrometry on 2 : 3 Ln : $H_2L^{C2'}$ stoichiometric solutions. Two main Ln-containing species with $[Ln_2(L^{C2'})_2]^{2+}$ and $[Ln_2(L^{C2'})_3]$ stoichiometry were evidenced for the metal ions studied, with the exception of Gd for which only the 2 : 3 species could be seen (Table 2). The latter species generate the most intense peaks in the spectra, except for Lu, and can be assigned to the triple-stranded bimetallic helicates, by reference to our earlier work[31,40,43] and on the basis of the experimental isotopic distributions which match the calculated ones (see Fig. S4, ESI† for examples). The 2 : 2 species has been observed previously, in particular when deciphering the formation mechanism of the parent $[Eu_2(L^C)_3]$ helicate in which it plays a key role.[28]

Conditional stability constants have been determined at pH 7.4 in Tris-HCl buffer by titrating $H_2L^{C2'}$ 1.06×10^{-5} M with concentrated solutions ($\approx 5 \times 10^{-3}$ M) of lanthanide perchlorates (Ln = La, Eu, Lu) for ratios $R = [Ln]_t/[H_2L^{C2'}]_t$ between 0 and 4. A typical example is shown on Fig. 2 (top). Factor analysis pointed to the presence of three (Eu, Lu) to four (La) species in solution. Several models were tested, but introduction of the 2 : 2 complex as one of the absorbing species invariably led to non-convergence of the least-squares fitting procedures. Therefore this species was removed from the models. The apparent discrepancy with ESI-MS data most probably arises from the larger concentration (about 40-fold) used for the latter experiments. The best convergence and smallest residuals are obtained when 1 : 2, 2 : 3 and 2 : 1 complexes are introduced into the model in the case of La (eqn (8)–(10), charges are omitted for clarity reasons), while for the two other metal ions, the model has to be abridged to two complex species only (1 : 2 and 2 : 3, eqn (8) and (9)).

$$2L^{C2'} + Ln \leftrightarrows [Ln(L^{C2'})_2]: \log \beta_{12} \quad (8)$$

$$3L^{C2'} + 2Ln \leftrightarrows [Ln_2(L^{C2'})_3]: \log \beta_{23} \quad (9)$$

$$L^{C2'} + 2Ln \leftrightarrows [Ln_2(L^{C2'})]: \log \beta_{21} \quad (10)$$

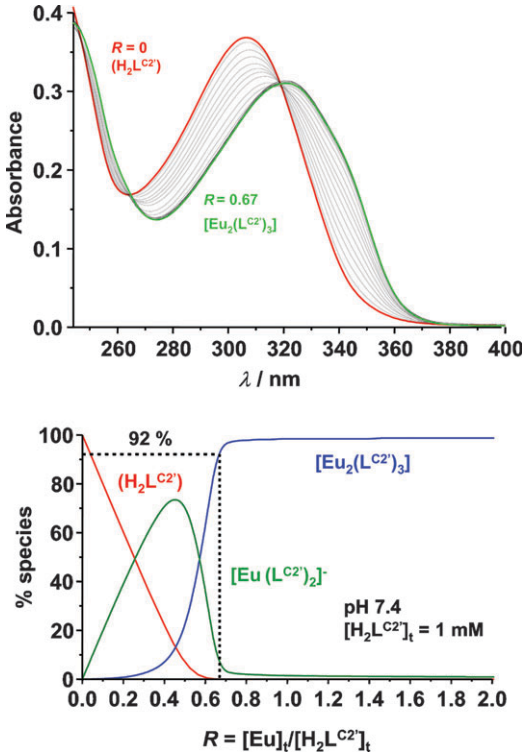

Fig. 2 (Top) Spectrophotometric titration of $H_2L^{C2'}$ 1.06×10^{-5} M in Tris-HCl 0.1 M by europium perchlorate at 298 K. (Bottom) Distribution diagram computed from the conditional stability constants listed in Table 3 for $[H_2L^{C2'}]_t = 1$ mM.

The recalculated spectra of the complexed species (Fig. S5, ESI,† Ln = Eu) are correlated which explains the difficulties encountered in the fitting procedure. In any case, as shown in Table 3 in which the corresponding conditional stability constants are listed, the 2 : 3 helicates are by large the most stable species in solution (see also Fig. 2, bottom). This is confirmed by the absorbance values extracted at different wavelengths which reach a constant value after $R = 0.67$ (see Fig. S6, ESI† for Ln = Eu).

The percentage of the Eu helicate for a millimolar total concentration in ligand (Table 3) is very similar to the one obtained for the corresponding helicates with the benzimidazole-substituted ligand H_2L^{C3}.[40] As a consequence, the present system, although not totally optimum from this point of view, can still be used for *in vitro* cell imaging experiments, especially that the free ligand and metal ion concentrations are quasi-negligible.

Photophysical properties

The unbound ligand presents two main absorption bands, one centred at 217 nm, with a shoulder at $\approx$230 nm, and the other at 307 nm; they are red-shifted to 220–222, $\approx$244, and 321–322 nm, respectively, upon formation of the helicates (Fig. S7, ESI†). Excitation into the $\pi \rightarrow \pi^*$ band of $H_2L^{C2'}$ at 307 nm results in the emission of a broad and intense peak centred at 392 nm, which disappears upon enforcement of a 0.05 ms time delay; it is therefore assigned to emission from singlet state(s). At 77 K, another band appears under time-resolved conditions, which extends from 400 to 625 nm, with a maximum at

Table 3 Conditional stability constants at pH 7.4 (see text), percentage of the 2 : 3 species for $[H_2L^{C2'}]_t = 10^{-3}$ M, and molar absorptivities of the ligand in the 2 : 3 species

Ln	$\log \beta_{12}$	$\log \beta_{23}$	$\log \beta_{21}$	% 2 : 3 species	$10^{-3}\varepsilon/M^{-1}\ cm^{-1}$	$10^{-3}\varepsilon^a/M^{-1}\ cm^{-1}$
La	14.8(1)	28.3(1)	13.8(2)	88	88.86	29.62
Eu	14.7(1)	28.0(1)	n.a.	92	89.31	29.77
Lu	14.4(4)	27.7(5)	n.a.	91	93.89	31.30

[a] Per molecule of ligand, compare, $\varepsilon = 35\,350\ M^{-1}\ cm^{-1}$ for uncomplexed $H_2L^{C2'}$.

Table 4 Energies (cm^{-1}) of the $^*\pi \leftarrow \pi$ transitions and of the singlet and triplet states for the ligand and its complexes at 295 K, and lifetime of the $^3\pi\pi^*$ state (τ in ms, at 77 K)

Species	$E_1(^*\pi \leftarrow \pi)$ ($\log \varepsilon$)	$E_2(^*\pi \leftarrow \pi)$ ($\log \varepsilon$)	$E(^1\pi\pi^*)^a$	$E(^3\pi\pi^*)^b$	τ (2σ)	$\Delta E(^1\pi\pi^*–^3\pi\pi^*)^c$
$(H_2L^{C2'})$	46 100 (4.83)	32 600 (4.55)	*25 500*	*20 350*, 21 150	428(11)	5150
$[La_2(L^{C2'})_3]$	45 050 (5.21)	31 150 (4.95)	*24 950*	*20 300*, 21 750	278(4)	4650
$[Eu_2(L^{C2'})_3]$	45 500 (5.17)	31 150 (4.92)	*25 700*	n.a.	n.a.	5400[d]
$[Gd_2(L^{C2'})_3]$	n.a.	n.a.	*24 900*	*19 100*, 21 900	10(1)	5800
$[Tb_2(L^{C2'})_3]$	45 500 (5.17)	31 100 (4.92)	*25 750*	n.a.	n.a.	5450[d]
$[Lu_2(L^{C2'})_3]$	45 500 (5.22)	31 000 (4.97)	*25 050*	*20 350*, 21 700	238(8)	4700

[a] From fluorescence spectra at 298 K (λ_{exc} = 307 and 321–323 nm), maximum of the band envelope. [b] From phosphorescence spectra at 77 K (λ_{exc} = 307 and 321–323 nm), maximum of the band envelope (italicized) and 0-phonon transition. [c] Calculated as the energy difference between the maxima of the band envelopes. [d] From $^3\pi\pi^*$ data for the La helicate.

493 nm and which is assigned to triplet state emission (Table 4). Little spectral shifts are seen upon complexation for both emission bands, but the lifetime of the triplet state is considerably shortened, particularly for the Gd^{III} helicate, a situation typically met for complexes with this 7/2-spin paramagnetic ion.[57] In addition, the phosphorescence band of the complexes with non-luminescent lanthanides clearly displays a four- to five-component vibrational progression with an average spacing of 1140 ± 30 (La), 1350 ± 90 (Gd), and 1240 ± 250 (Lu) cm^{-1}, corresponding to a ring breathing mode of the ligand strands (Fig. S8, ESI†).

At room temperature, the ligand singlet state emission almost completely disappears for the helicates with luminescent Eu^{III} and Tb^{III} ions and the characteristic line-like phosphorescence from the Eu($^5D_0$) and Tb($^5D_4$) levels dominates the spectra (Fig. 3). It is worth noting that the excitation spectra of the Eu^{III} and Tb^{III} helicates match the corresponding absorption spectra, a definite proof of the ligand-to-metal energy transfer.

One of the privileged energy migration pathways involves an initial fast singlet-to-triplet (intersystem crossing, isc) step, as exemplified by the very weak remaining singlet-state emission: 2% and 4% of the unbound ligand fluorescence for Eu^{III} and Tb^{III}, respectively. The rate constant of the isc process is therefore quite large ($k_{isc} > k_{fluor}$), reflecting the favourable energy difference between the singlet and triplet states, ≈5000 cm^{-1} (Table 4).[58] The second step in the transfer process ($^3\pi\pi^*$-to-Ln) appears to be very efficient since no residual ligand phosphorescence is observed at 77 K. Moreover, the lifetime of the ligand triplet state is considerably shortened in the complexes, from 428 ms for the unbound ligand to 10 ms for the Gd^{III} helicate.

The inner coordination sphere of the metal ions has been probed by high-resolution luminescence data recorded on a frozen (10 K) aqueous solution of $[Eu_2(L^{C2'})_3]$ 2.5×10^{-4} M (Fig. S9, ESI†). The emission spectrum can be interpreted as arising from a main species with a distorted D_3 symmetry. First, the 0–0 transition is weak (0.5% of the total $^5D_0$ emission), reasonably narrow (full width at half height = 15 cm^{-1}), and its energy (17 233 cm^{-1}) matches fairly well the theoretical value (17 231 cm^{-1}) calculated from a phenomenological equation with the following nephelauxetic parameters:[59] $\delta_{carb} = -17.2\ cm^{-1}$ for the carboxylates and $\delta_{bzp} = -15.3\ cm^{-1}$ for the heterocyclic nitrogen donors.[60] Secondly, the $^5D_0 \rightarrow {}^7F_1$ transition is split into two main bands,

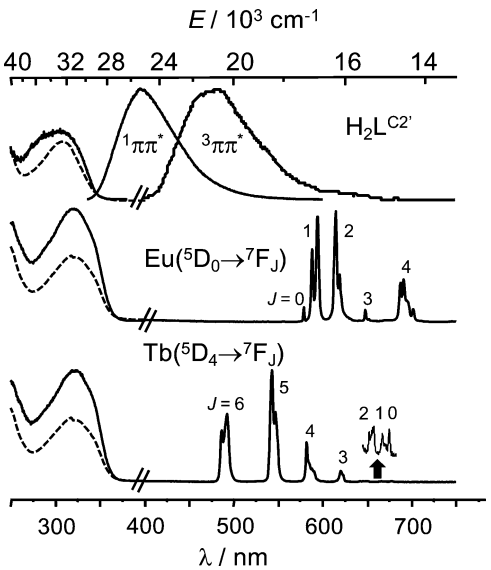

Fig. 3 Normalized absorption (left, dotted lines), excitation (left, solid lines), and emission (right) spectra of the unbound ligand (top) and of its Eu (middle; the very weak transitions to $^7F_5$ and $^7F_6$ are not shown) and Tb (bottom) helicates, at 298 K (except for the $^3\pi\pi^*$ emission, 77 K, time delay 0.05 ms); aqueous solutions at pH 7.4 (Tris-HCl 0.1 M), $[H_2L^{C2'}]_{tot} = 4.5 \times 10^{-5}$ M; excitation wavelength: 307 nm (ligand) and 321 nm (helicates).

Table 5 Quantum yields (±10%), ^5D_J lifetimes (ms), and hydration numbers[62,63] for $[Ln_2(L^{CX})_3]$ helicates 10–15 μM in Tris-HCl 0.1 M, determined under ligand excitation[a]

Compound	Q^L_{Ln} (%)	τ(H_2O)/ms	τ(D_2O)/ms	q (±0.3)
$[Eu_2(L^C)_3]$	24	2.43 ± 0.01	4.66 ± 0.02	0.2
$[Eu_2(L^{C2})_3]$	21	2.43 ± 0.09	4.38 ± 0.04	−0.1
$[Eu_2(L^{C2'})_3]$	19	2.43 ± 0.03	4.22 ± 0.07	−0.1
$[Tb_2(L^C)_3]$	1.2	0.050 ± 0.005	n.a.	n.a.
$[Tb_2(L^{C2})_3]$	11	0.65 ± 0.02	0.94 ± 0.02	[b]
	n.a.	2.58 ± 0.05[c]	2.67 ± 0.04[c]	−0.2[c]
$[Tb_2(L^{C2'})_3]$	10	0.66 ± 0.02	1.05 ± 0.06	[b]
	n.a.	2.58 ± 0.09[c]	2.7 ± 0.2[c]	−0.2[c]

[a] Data for helicates with H_2L^C and H_2L^{C2} are from refs. 31, 41 and 43. [b] Equations not applicable. [c] At 77 K.

assigned to transitions to the A($^7F_1$) and E($^7F_1$) ligand-field sublevels. The latter is further split into two components. In axial symmetry, the ΔE(A–E) energy splitting (161 cm^{-1}) is directly proportional to the B_0^2 ligand-field parameter, which can estimated to be −600 cm^{-1}.[61] Furthermore, the ΔE(E–E) separation is indicative of the extent of distortion from the idealized D_3 symmetry; it amounts to 31 cm^{-1}. These energy differences are exactly the same as those reported for the Eu^{III} helicate with shorter polyoxyethylene chains, $[Eu_2(L^{C2})_3]$[43] and very similar to the ones found for the parent helicate $[Eu_2(L^C)_3]$ (156 and 28 cm^{-1}, respectively) for which a crystal structure indicates moderate distortion from D_3.[31] When measured under high-resolution conditions, the Eu($^5D_0$) decay is a bi-exponential function, from which two lifetimes can be extracted: a long one (2.36 ± 0.01 ms, population 94%) assigned to the N_6O_3 environment found in the 2 : 3 helicate, and a shorter one (0.89 ± 0.03 ms) corresponding to a minor species (6%) with one coordinated water molecule. This reflects the speciation unravelled by the other spectroscopic techniques, but the population of this species is too small to affect substantially the emission spectrum and therefore to identify it unambiguously.

The quantum yields are reported in Table 5, along with lifetime data and calculated hydration numbers.[62,63] It is noteworthy that the lengthening of the polyoxyethylene pendant arms has little influence on these data. The quantum yields decrease by about 10% while the Eu($^5D_0$) lifetimes are exactly the same for the three related helicates with H_2L^C, H_2L^{C2}, and $H_2L^{C2'}$ and temperature-independent down to 10 K.

The hydration numbers for the Eu^{III} chelates are essentially zero, within the accuracy of the phenomenological equations, which means that given the above analysis, the inner coordination sphere of the lanthanide ion is very similar in the three helicates and corresponds to the sketch shown at the bottom of Scheme 1. The temperature dependence of the Tb($^5D_4$) lifetime is quite large, which is indicative of a back transfer process taking place between the ligand triplet state and the $^5D_4$ level. This is in line with the relatively small energy gap between the emitting level and the 0-phonon level of the triplet state (taken as being the same as for the Gd^{III} helicate), $\Delta E(^3\pi\pi^*(0)–^5D_4)$ = 1400 cm^{-1}, which can easily be bridged by a single vibrational phonon. Under these conditions, the equations for estimating the hydration number q are not valid since they are based on the assumption that quenching by O–H is the only important non-radiative deactivation process operating in the chelate. When the hydration number is calculated with lifetime data recorded at 77 K, a temperature at which the phonon-assisted back transfer is minimized,[43] its value is indeed close to zero.

The ligand sensitization ability can be estimated for the Eu^{III} helicate by the following equation:[64]

$$\eta_{sens} = \frac{Q^L_{Eu}}{Q^{Eu}_{Eu}} = Q^L_{Eu}\frac{\tau_{rad}}{\tau_{obs}} = \frac{Q^L_{Eu}}{\tau_{obs}}\left(\frac{I_{MD}}{I_{tot}}\right)\frac{1}{A_{MD,0}n^3} \qquad (11)$$

where Q^{Eu}_{Eu} is the intrinsic quantum yield (*i.e.* the quantum yield obtained by direct metal excitation) which reflects the extent of non-radiative de-activation processes, τ_{obs} is the observed lifetime, τ_{rad} the radiative lifetime, I_{MD} the integrated intensity of the purely magnetic dipole transition $^5D_0 \rightarrow {}^7F_1$, I_{tot} the integrated intensity of the entire emission spectrum, n the refractive index (1.334 for H_2O), and $A_{MD,0}$ is a rate constant independent of the Eu^{III} environment, equal to 14.65 s^{-1}. The radiative lifetime amounts to 6.6 ms, as compared to 6.9 ms for $[Eu_2(L^{C2})_3]$, leading to an intrinsic quantum yield equal to 36.6%, as compared to 36.4% for $[Eu_2(L^{C2})_3]$, which means that the decrease in the overall quantum yield observed upon lengthening the polyoxyethylene chain is traced back to a less efficient ligand-to-metal energy transfer, η_{sens} decreasing from 58 to 52%. The corresponding data for the unsubstituted helicate $[Ln_2(L^C)_3]$ are 7.1 ms, 36.7% and 67%, respectively. Therefore, the non-radiative de-activation processes operating in the inner coordination sphere of the three helicates are very similar and not affected by the substitution on the pyridine 4-position. On the other hand, the ligand-to-metal energy transfer process is sensitive to this substitution, η_{sens} decreasing by 13% in going from R^2 = H to R^2 = $(OCH_2CH_2)_3OMe$ and by 10% in going from the latter to R^2 = $(OCH_2CH_2)_6OMe$.

Live cell imaging

HeLa cells grown on glass bottom cell culture dishes were incubated in cell culture medium with $[Eu_2(L^{C2'})_3]$ at different concentrations. Cells were examined with a luminescence microscope 7 h after complex loading. The helicate clearly permeates into HeLa cells and stains their cytoplasm in a concentration dependent manner, the higher the concentration, the brighter the images. Loading concentrations down to 10 μM showed distinct luminescent images of the cells (Fig. 4, top). Counter-staining experiments were undertaken to confirm the cell localization of $[Eu_2(L^{C2'})_3]$ in the cytoplasm. Live cells were loaded with the complex and the commercially available nucleus stain acridine orange and examined by microscopy using the appropriate filters (Fig. 4, bottom). We could clearly observe the red emission of the helicate in the cytoplasm of the cells and the green acridine orange emission in the nucleus (note that for cancerous cells, the nucleus is unusually large).

A key question is whether the cells remain viable and healthy over the period of examination. Therefore the influence of the $[Eu_2(L^{C2'})_3]$ helicate on cell proliferation and viability was examined by the WST-1 assay[54,55] at time

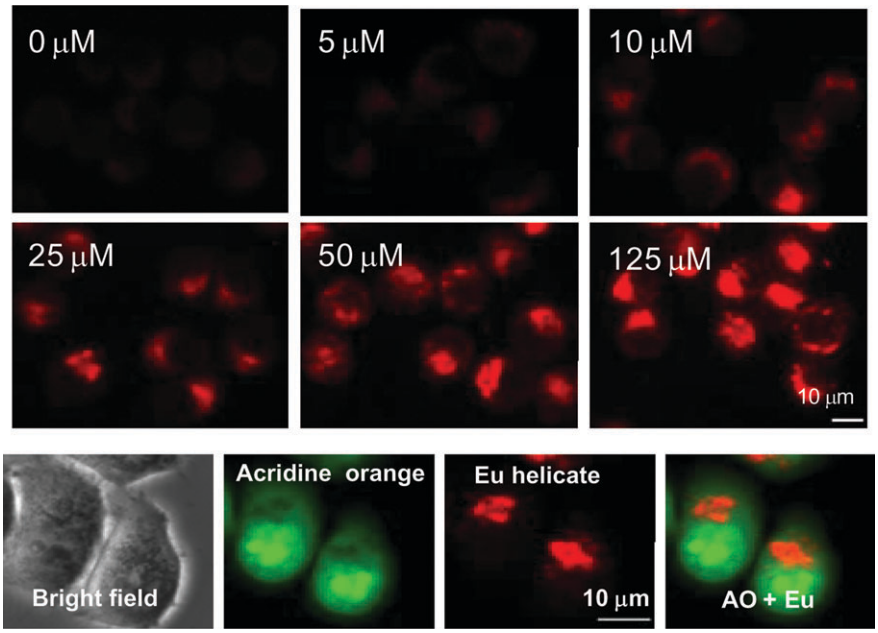

Fig. 4 (Top) Luminescence images of HeLa cells loaded with different concentrations of $[Eu_2(L^{C2'})_3]$ in RPMI-1640 for 7 h at 37 °C. The images were taken with a Zeiss luminescence microscope Axiovert S100 (Objective: Plan-Neofluar, 20×; λ_{exc} = 330 nm, emission filter = LP 585 filter, exposure time 60 s). (Bottom) Images of HeLa cells loaded with 250 μM $[Eu_2(L^{C2'})_3]$ (5 h at 37 °C), then incubated with 40 μg ml^{-1} acridine orange in PBS (5 min at rt), and washed 10× with PBS. The images were taken as above for Eu^{III} (exposure time 10 s) and at λ_{exc} = BP 450–490 nm with an emission filter BP 515–565 nm, exposure time 10 ms, for acridine orange.

intervals in the range of 30 min to 24 h. As shown in Fig. S10, left (ESI† left), no significant difference can be observed between the proliferation of HeLa cells in absence or presence of the helicate up to 500 μM. This observation is confirmed by the viability of the cells after 24 h of incubation with $[Eu_2(L^{C2'})_3]$ (Fig. S10, right, ESI†): 100% for 0 μM, 101 ± 1% for 125 μM, 99 ± 2% for 250 μM, and 101 ± 1% for 500 μM. The time course and temperature dependence of the complex loading were determined in order to unravel the mechanism by which the cells take up the helicate. The HeLa cells were incubated with a 500 μM solution of $[Eu_2(L^{C2'})_3]$ in cell culture medium at 37 °C and examined by luminescence microscopy from 15 min to 24 h after complex loading. The first bright spots in the cytoplasm of the cells can be observed as early as 15 min after incubation (Fig. S11, ESI†). The presence of vesicular structures in the cytoplasm of the cells is supportive of an endocytotic uptake mechanism. Since it is known that such a mechanism can be blocked at 4 °C, the cells were loaded with a 100 μM solution of the $[Eu_2(L^{C2'})_3]$ complex in cell culture medium at 4 °C for 7 h, in a separate experiment. No europium luminescence could be observed at 4 °C, indicating that the helicate is likely to enter the cells by endocytosis (Fig. S12, ESI†). This observation is further confirmed by co-localization experiments in which live cells were loaded simultaneously with the Eu^{III} helicate and one commercially available marker for endocytosis, namely BIODIPY FL labelled transferrin or LDL. The subsequent luminescence images taken using appropriate filters reveal that a vast majority of compartments which internalize the helicate also contain the organic marker (Fig. 5, third column), as evidenced by the appearance of bright yellow spots (Fig. 5, fourth column) after merging the images. In addition, nearly all the endocytosed helicates are internalized in receptor-containing vesicles. These observations strongly suggest the uptake of the complex *via* a lysosomally directed and/or a recycling endosomal pathway.

In order to estimate the intracellular concentration of the helicate, the europium concentration was measured in a given cell cohort with the Delfia® method after incubation overnight with 25 μM of the helicate.[65] A suitable calibration curve was established (Fig. S13, ESI†) from which it was deduced that under the loading conditions used, each cell contains on average 8.8×10^{-16} mol of $[Eu_2(L^{C2'})_3]$. Taking into account that the volume of a HeLa cell lies between 2.6×10^3 μm^3 and 4.2×10^3 μm^3, as estimated from the cell diameter measured under the microscope, this translates into an intracellular concentration between 0.21 and 0.34 μM.

The question arises whether or not the helicate survives un-dissociated in the cells at such low concentrations. To address this problem, the emission spectrum of the internalized helicate is compared on Fig. 6 with the spectrum of a solution in RPMI cell culture medium. The two spectra are very similar, as demonstrated by the identical ligand-field splittings and by the intensity ratios $I(^5D_0 \rightarrow {}^7F_J)/I(^5D_0 \rightarrow {}^7F_1)$: 0.015, 1.00, 1.25, 0.12, 2.06, 0.06 in RPMI-1640 for J = 0–5, as compared to 0.016, 1.00, 1.18, 0.12, 1.88, and 0.05, respectively, *in cellulo*. While the luminescence decay is a single exponential in the cell culture medium, corresponding to a $Eu(^5D_0)$ lifetime of 2.31 ± 0.03 ms, it has to be analyzed in terms of a bi-exponential function *in cellulo*, with associated lifetimes of 2.20 ± 0.03 ms and 0.48 ± 0.06 ms. The longer lifetime is only marginally smaller than the one measured in Tris-HCl (−9%) and in RPMI-1640 (−5%), and the related species has a population of 93%. The shorter

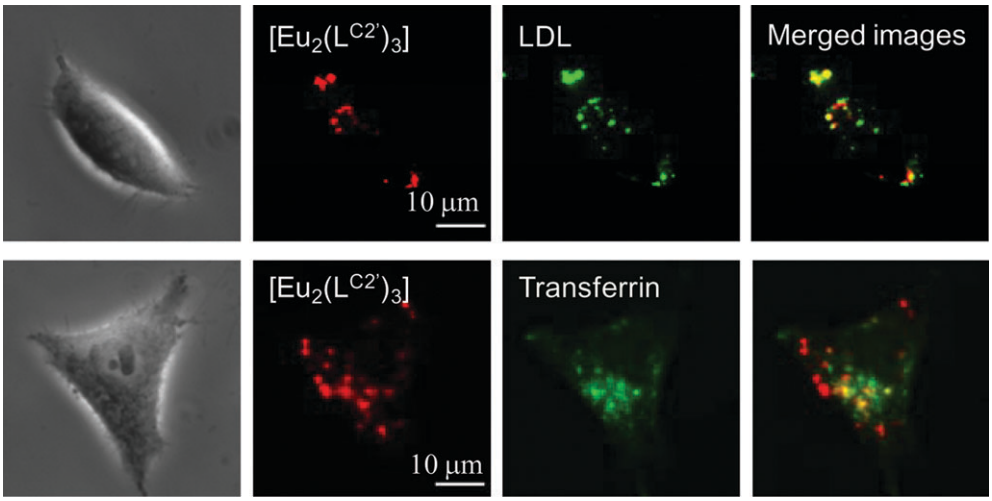

Fig. 5 Co-localization experiments: cells loaded with $[Eu_2(L^{C2'})_3]$ 250 μM and 15 μg ml^{-1} BIODIPY FL LDL (0.5 h, top) or 50 μg ml^{-1} BIODIPY FL transferrin (2 h bottom). First column: bright field images; second column: Eu^{III} luminescence (λ_{exc} = 330 nm, 60 s exposure time); third column BIODIPY FL labelled LDL (λ_{exc} = 470 nm, 2 s exposure time) or BIODIPY FL labelled transferrin (λ_{exc} = 470 nm, 3 s exposure time); fourth column, merged images.

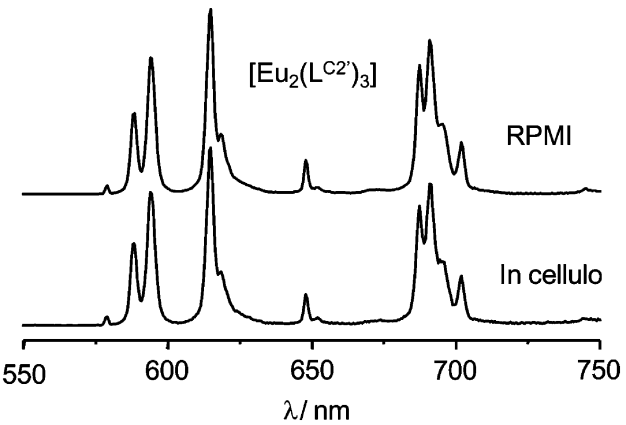

Fig. 6 Emission spectra of $[Eu_2(L^{C2'})_3]$ 125 μM in RPMI-1640 (top) and *in cellulo* (HeLa cells incubated overnight with 250 μM $[Eu_2(L^{C2'})_3]$); λ_{exc} = 321 nm.

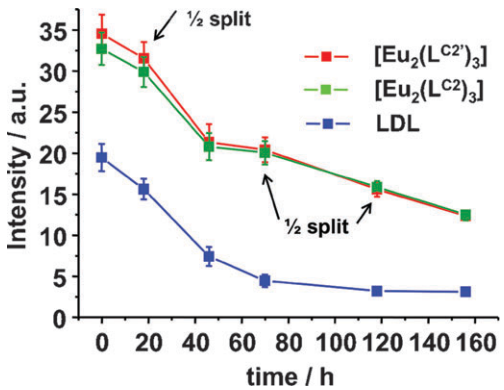

Fig. 7 Leakage of $[Eu_2(L^{C2'})_3]$ and $[Eu_2(L^{C2})_3]$ from HeLa cells *vs.* time. Cells were incubated 6 h at 37 °C with 100 μM of helicate or 2 h at 37 °C with 10 μg/ml of BIODIPY FL labeled LDL. Cultures were then maintained at 37 °C under 5% CO_2 and cells were split every 48 h.

lifetime is typical of an Eu^{III} species containing approximately two water molecules in the inner coordination sphere which could arise from partial dissociation of one ligand strand; the population of this species is, however quite small, so that it is not detrimental to the use of $[Eu_2(L^{C2'})_3]$ as cell staining agent. As a comparison, the luminescence decay for $[Eu_2(L^{C2})_3]$ was a single exponential function, but the reported $Eu(^5D_0)$ lifetime was substantially smaller (1.6 ± 0.2 ms).

Finally, the leakage of the Eu^{III} helicates out of the HeLa cells has been monitored as follows (Fig. 7). The cells were loaded with one of the chelates and LDL as control. After adequate washing, the total emitted intensity was monitored over 20 h while maintaining the culture conditions; an intensity loss of less than 10% was recorded after 20 h for both $[Eu_2(L^{C2})_3]$ and $[Eu_2(L^{C2'})_3]$ helicates, which was slightly less than the loss experienced by LDL. At that stage, the cells were split into two equal samples (1/2 split) and one of them examined under the microscope after a 20 h incubation time. The experiment was repeated every other day. Again, very little leakage is seen for both helicates, the luminescence intensity decreasing approximately by half, as expected, with each cell division.

Conclusion

The lengthening of the polyoxyethylene chains grafted in R^2 in going from H_2L^{C2} to $H_2L^{C2'}$ only marginally affects the thermodynamic and photophysical properties of the $[Ln_2(L^{C2'})_3]$ helicates, which remain quite stable in aqueous solution at pH 7.4. The proportion of the Eu^{III} helicate with $H_2L^{C2'}$ is 92% at a millimolar total ligand concentration, as compared to 98% for H_2L^{C2}. Another small change is the 10% decrease in the overall quantum yield. Interestingly, this decrease can be traced back to a less efficient ligand-to-metal energy transfer, despite a slightly longer lifetime of the triplet state of the helicates with paramagnetic Ln^{III} ions (*e.g.* 10 *vs.* 8.7 ms for the Gd^{III} helicates). On the other hand, non-

radiative de-activation processes remain quite comparable in the two classes of helicates, as shown by identical intrinsic quantum yields for Eu^{III}. That is, the inner coordination sphere is not influenced by the ligand modification.

Comparing $[Eu_2(L^{C2'})_3]$ with $[Eu_2(L^{C2})_3]$ does not reveal any significant difference in cell imaging properties either: same concentration dependence (Fig. S14, ESI†), same time course (Fig. S15, ESI†), same mechanism of uptake—endocytosis, very similar average cellular concentration (0.28 μM for $[Eu_2(L^{C2'})_3]$ as compared to 0.25 μM for $[Eu_2(L^{C2})_3]$,[43] and, finally, identical behaviour towards cell leakage, *i.e.* negligible over three splits and 160 h.

Therefore, contrary to the cyclam complex cited in the introduction, for which a minor change in the length of one substituent, namely the addition of one methylene group, leads to important modifications of its biological activity,[44] the chemical and biochemical properties of the $[Ln_2(L^{CX})_3]$ helicates remain rather insensitive to the substitution in the pyridine 4-position. This is very encouraging for the targeting experiments we are planning to conduct in a near future and which require modification of the tris(polyoxyethylene) pendant arms of H_2L^{C2}, as well as, in some instances, a lengthening of the functionalized arm to avoid close contact between the emissive stain and the targeted biological site. Furthermore, the data on cell leakage reported here comfort our opinion that $[Ln_2(L^{CX})_3]$ helicates are a viable alternative to existing chelates reported in the literature for bio-medical analyses and imaging.[41]

Acknowledgements

This work is supported through grants from the Swiss National Science Foundation (200020-119866/1) and the Swiss Secretariat for Education and Research (project C07.0116). Selected funding from the European Science Foundation through COST action D38 is also acknowledged. We thank Frédéric Gumy for his help with the measurement of high resolution luminescence data and quantum yields as well as Steve Comby for his advice regarding spectrophotometric titrations and luminescence measurements.

References

1. N. Johnsson and K. Johnsson, *ACS Chem. Biol.*, 2007, **2**, 31.
2. A. Loudet and K. Burgess, *Chem. Rev.*, 2007, 4891.
3. S. M. J. Dunn, in *Handbook of Neurochemistry and Molecular Neurobiology: Practical Neurochemical Methods*, ed. A Lajtha, Springer Verlag, Berlin, 2007, pp. 133–48.
4. R. A. Poole, G. Bobba, M. J. Cann, J. C. Frias, D. Parker and R. D. Peacock, *Org. Biomol. Chem.*, 2005, **3**, 1013.
5. R. Créton, J. A. Kreiling and L. F. Jaffe, *Microsc. Res. Technol.*, 2007, **46**, 390.
6. J. Inglese, R. L. Johnson, A. Simeonov, M. H. Xia, W. Zheng, C. P. Austin and D. S. Auld, *Nat. Chem. Biol.*, 2007, **3**, 466.
7. R. Weissleder and V. Ntziachristos, *Nat. Med.*, 2003, **9**, 123.
8. J.-C. G. Bünzli, in *Lanthanide Probes in Life, Chemical and Earth Sciences. Theory and Practice*, ed. J.-C. G. Bünzli and G. R. Choppin, Elsevier Science Publ. B.V., Amsterdam, 1989, ch. 7, pp. 219–293.
9. J.-C. G. Bünzli, *Acc. Chem. Res.*, 2006, **39**, 53.
10. M. Ferrer, P. Zuck, G. Kolodin, S. S. Mao, R. R. Peltier, C. Bailey, S. J. Gardell, B. Strulovici and J. Inglese, *Anal. Biochem.*, 2003, **317**, 94.
11. K. Hanaoka, K. Kikuchi, S. Kobayashi and T. Nagano, *J. Am. Chem. Soc.*, 2007, **129**, 13502.
12. I. Hemmilä and V. M. Mukkala, *Crit. Rev. Clin. Lab. Sci.*, 2001, **38**, 441.
13. V. W. W. Yam and K. K. W. Lo, *Coord. Chem. Rev.*, 1999, **184**, 157.
14. S. Faulkner and J. L. Matthews, in *Comprehensive Coordination Chemistry II*, ed. M. D. Ward, Elsevier Pergamon, Amsterdam, 2004, ch. 9.21, vol. 9, pp. 913–44.
15. S. Comby and J.-C. G. Bünzli, in *Handbook on the Physics and Chemistry of Rare Earths*, ed. K. A. Gschneidner, Jr, J.-C. G. Bünzli and V. K. Pecharsky, Elsevier Science B.V., Amsterdam, 2007, ch. 235, vol. 37.
16. R. Weissleder, *Nat. Biotechnol.*, 2001, **19**, 316.
17. S. Phimphivong and S. S. Saavedra, *Bioconjugate Chem.*, 1998, **9**, 350.
18. S. Pandya, J. H. Yu and D. Parker, *Dalton Trans.*, 2006, 2757.
19. J. H. Yu, D. Parker, R. Pal, R. A. Poole and M. J. Cann, *J. Am. Chem. Soc.*, 2006, 2294.
20. R. Pal and D. Parker, *Chem. Commun.*, 2007, 474.
21. R. A. Poole, C. P. Montgomery, E. J. New, A. Congreve, D. Parker and M. Botta, *Org. Biomol. Chem.*, 2007, **5**, 2055.
22. M. Albrecht, *Chem. Rev.*, 2001, **101**, 3457.
23. J.-M. Lehn, *Proc. Natl. Acad. Sci. USA*, 2002, **99**, 4763.
24. L. J. Martin, M. J. Hahnke, M. Nitz, J. Wohnert, N. R. Silvaggi, K. N. Allen, H. Schwalbe and B. Imperiali, *J. Am. Chem. Soc.*, 2007, **129**, 7106.
25. C. Piguet, E. Rivara-Minten, G. Hopfgartner and J.-C. G. Bünzli, *Helv. Chim. Acta*, 1995, **78**, 1651.
26. J.-C. G. Bünzli and C. Piguet, *Chem. Rev.*, 2002, **102**, 1897.
27. M. Elhabiri, J. Hamacek, N. Humbert, J.-C. G. Bünzli and A.-M. Albrecht-Gary, *New J. Chem.*, 2004, **28**, 1096.
28. M. Elhabiri, J. Hamacek, J.-C. G. Bünzli and A.-M. Albrecht-Gary, *Eur. J. Inorg. Chem.*, 2004, 51.
29. M. Cantuel, G. Bernardinelli, G. Muller, J. P. Riehl and C. Piguet, *Inorg. Chem.*, 2004, **43**, 1840.
30. M. Albrecht, S. Schmid, S. Dehn, C. Wickleder, Z. Shuang, A. P. Bassett, Z. Pikramenou and R. Fröhlich, *New J. Chem.*, 2007, **31**, 1755.
31. M. Elhabiri, R. Scopelliti, J.-C. G. Bünzli and C. Piguet, *J. Am. Chem. Soc.*, 1999, **121**, 10747.
32. J.-C. G. Bünzli, in *Rare Earths*, eds. R Saez Puche and P Caro, Editorial Complutense, Madrid, 1998, pp. 223–59.
33. E. Moret, F. Nicolo, J.-C. G. Bünzli and G. Chapuis, *J. Less-Common Met.*, 1991, **171**, 273.
34. N. André, T. B. Jensen, R. Scopelliti, D. Imbert, M. Elhabiri, G. Hopfgartner, C. Piguet and J.-C. G. Bünzli, *Inorg. Chem.*, 2004, **43**, 515.
35. T. B. Jensen, R. Scopelliti and J.-C. G. Bünzli, *Inorg. Chem.*, 2006, **45**, 7806.
36. T. B. Jensen, R. Scopelliti and J.-C. G. Bünzli, *Chem.–Eur. J.*, 2007, 8404.
37. T. B. Jensen, R. Scopelliti and J.-C. G. Bünzli, *Dalton Trans.*, 2008, 1027.
38. C. Piguet, E. Rivara-Minten, G. Hopfgartner and J.-C. G. Bünzli, *Helv. Chim. Acta*, 1995, **78**, 1541.
39. M. Elhabiri, R. Scopelliti, J.-C. G. Bünzli and C. Piguet, *Chem. Commun.*, 1998, 2347.
40. A.-S. Chauvin, S. Comby, B. Song, C. D. B. Vandevyver and J.-C. G. Bünzli, *Chem.–Eur. J.*, 2007, **13**, 9515.
41. J.-C. G. Bünzli, A.-S. Chauvin, C. D. B. Vandevyver, B. Song and S. Comby, *Ann. N. Y. Acad. Sci.*, 2008, DOI: 10.1196/annals.1430.010.
42. C. D. B. Vandevyver, A.-S. Chauvin, S. Comby and J.-C. G. Bünzli, *Chem. Commun.*, 2007, 1716.
43. A.-S. Chauvin, S. Comby, B. Song, C. D. B. Vandevyver and J.-C. G. Bünzli, *Chem.–Eur. J.*, 2008, **14**, 1726.
44. K. J. Heroux, K. S. Woodin, D. J. Tranchemontagne, E. Southwick, E. H. Wong, G. R. Weisman, S. A. Tomellini, T. J. Wadas, C. J. Anderson, S. Kassel, J. A. Golen and A. L. Rheingold, *Dalton Trans.*, 2007, 2150.
45. A. B. Pangborn, M. A. Giardello, R. H. Grubbs, R. K. Rosen and F. J. Timmers, *Organometallics*, 1996, **15**, 1518.
46. C. Piguet, G. Bernardinelli, B. Bocquet, A. Quattropani and A. F. Williams, *J. Am. Chem. Soc.*, 1992, **114**, 7440.

47. J.-C. G. Bünzli and C. Mabillard, *Inorg. Chem.*, 1986, **25**, 2750.
48. G. Schwarzenbach, *Complexometric Titrations*, Chapman & Hall, London, 1957.
49. K. N. Raymond, *Chem. Eng. News*, 1983, **61**, 4.
50. E. R. Malinowski and D. G. Howery, *Factor Analysis in Chemistry*, John Wiley, New York, Chichester, Brisbane, Toronto, 1991.
51. H. Gampp, M. Maeder, C. J. Meyer and A. D. Zuberbühler, *Talanta*, 1986, **33**, 943.
52. R. Rodriguez-Cortinas, F. Avecilla, C. Platas-Iglesias, D. Imbert, J.-C. G. Bünzli, A. de Blas and T. Rodriguez-Blas, *Inorg. Chem.*, 2002, **41**, 5336.
53. F. Gumy, *Int. Pat. Appl.*, 0013-066.B.WO, 2007.
54. M. Ishiyama, M. Shiga, K. Sasamoto, M. Mizoguchi and P. G. He, *Chem. Pharm. Bull.*, 1993, **41**, 1118.
55. M. Ishiyama, K. Sasamoto, M. Shiga, Y. Ohkura, K. Ueno, K. Nishiyama and I. Taniguchi, *Analyst*, 1995, **120**, 113.
56. M. A. Phillips, *J. Chem. Soc.*, 1928, 172.
57. S. Tobita, M. Arakawa and I. Tanaka, *J. Phys. Chem.*, 1985, **89**, 5649.
58. F. J. Steemers, W. Verboom, D. N. Reinhoudt, E. B. Vandertol and J. W. Verhoeven, *J. Am. Chem. Soc.*, 1995, **117**, 9408.
59. S. T. Frey and W. d. Horrocks, Jr, *Inorg. Chim. Acta*, 1995, **229**, 383.
60. C. Piguet, J.-C. G. Bünzli, G. Bernardinelli, G. Hopfgartner, S. Petoud and O. Schaad, *J. Am. Chem. Soc.*, 1996, **118**, 6681.
61. C. Görller-Walrand and K. Binnemans, in *Handbook on the Physics and Chemistry of Rare Earths*, ed. K. A. Gschneidner, Jr and L Eyring, Elsevier Science B.V., Amsterdam, 1996, ch. 155, vol. 23.
62. R. M. Supkowski and W. d. Horrocks, Jr, *Inorg. Chim. Acta*, 2002, **340**, 44.
63. A. Beeby, I. M. Clarkson, R. S. Dickins, S. Faulkner, D. Parker, L. Royle, A. S. de Sousa, J. A. G. Williams and M. Woods, *J. Chem. Soc., Perkin Trans. 2*, 1999, 493.
64. M. H. V. Werts, R. T. F. Jukes and J. W. Verhoeven, *Phys. Chem. Chem. Phys.*, 2002, **4**, 1542.
65. I. Hemmilä, T. Ståhlberg and P. Mottram, *Bioanalytical Applications of Labelling Technologies*, Wallac Oy, Turku, 1995.

